Molecular Therapy
Nucleic Acids
Original Article

Deficiency of miR-409-3p improves myocardial neovascularization and function through modulation of DNAJB9/p38 MAPK signaling

Furkan Bestepe,[1,7] Colette Fritsche,[1,7] Kartik Lakhotiya,[1] Carolyn E. Niosi,[1] George F. Ghanem,[1] Gregory L. Martin,[1] Ruma Pal-Ghosh,[1] Dakota Becker-Greene,[2] James Weston,[1] Ivana Hollan,[3] Ivar Risnes,[4] Stein Erik Rynning,[5] Liv Heidi Solheim,[6] Mark W. Feinberg,[2] Robert M. Blanton,[1] and Basak Icli[1]

[1]Molecular Cardiology Research Institute, Department of Medicine, Tufts Medical Center, Boston, MA 02111, USA; [2]Cardiovascular Division, Department of Medicine, Brigham & Women's Hospital, Harvard Medical School, Boston, MA 02115, USA; [3]Department of Health Sciences, Norwegian University of Science and Technology, Gjøvik, Norway; [4]Department of Cardiac Surgery, LHL Hospital Gardermoen, Jessheim, Norway; [5]Department of Heart Diseases, Haukeland University Hospital, Bergen, Norway; [6]HMN Lan & Helseplattformen, Trondheim, Norway

Angiogenesis is critical for tissue repair following myocardial infarction (MI), which is exacerbated under insulin resistance or diabetes. MicroRNAs are regulators of angiogenesis. We examined the metabolic regulation of miR-409-3p in post-infarct angiogenesis. miR-409-3p was increased in patients with acute coronary syndrome (ACS) and in a mouse model of acute MI. In endothelial cells (ECs), miR-409-3p was induced by palmitate, while vascular endothelial growth factor (VEGF) and fibroblast growth factor (FGF) decreased its expression. Overexpression of miR-409-3p decreased EC proliferation and migration in the presence of palmitate, whereas inhibition had the opposite effects. RNA sequencing (RNA-seq) profiling in ECs identified DNAJ homolog subfamily B member 9 (DNAJB9) as a target of miR-409-3p. Overexpression of miR-409-3p decreased DNAJB9 mRNA and protein expression by 47% and 31% respectively, while enriching DNAJB9 mRNA by 1.9-fold after Argonaute2 microribonucleoprotein immunoprecipitation. These effects were mediated through p38 mitogen-activated protein kinase (MAPK). Ischemia-reperfusion (I/R) injury in EC-specific *miR-409-3p* knockout (KO) mice (miR-409^{ECKO}) fed a high-fat, high-sucrose diet increased isolectin B4 (53.3%), CD31 (56%), and DNAJB9 (41.5%). The left ventricular ejection fraction (EF) was improved by 28%, and the infarct area was decreased by 33.8% in miR-409^{ECKO} compared with control mice. These findings support an important role of *miR-409-3p* in the angiogenic EC response to myocardial ischemia.

INTRODUCTION

Acute myocardial infarction (MI) is characterized by myocardial necrosis following coronary artery occlusion, resulting in prolonged myocardial ischemia.[1,2] Over the past several decades, patient survival rates and recurrent ischemic event rates post MI have improved because of recent advances in pharmacological management and interventions.[3] However, long-term morbidity and mortality after acute MI remains high because of left ventricular (LV) dysfunction and adverse LV remodeling, consisting of myocardial fibrosis and cardiac hypertrophy.[2,4] Post-MI healing requires angiogenesis early in the process, beginning in the border zone. Stimulation of this response to enhance extension of newly formed blood vessels into the infarcted zone is associated with improved outcomes consisting of less remodeling, improved heart function, and reduced infarct size in animal models. These observations indicate that improving the natural angiogenic response post MI might represent a therapeutic strategy.[2] However, diabetes impairs the angiogenic response and post-MI reparative process in human and animal models.[5–7]

Angiogenesis is the formation of new blood vessels from preexisting vessels. In this highly regulated process, activated endothelial cells (ECs) proliferate, migrate, and differentiate to form a new vascular lumen in response to proangiogenic stimuli such as vascular endothelial growth factor (VEGF), fibroblast growth factor (FGF), or tumor necrosis factor alpha (TNF-α).[8] After an ischemic event in the heart, proangiogenic factors are induced to stimulate blood flow to the infarcted region of the myocardium. Current investigational treatments focus on use of proangiogenic and anti-apoptotic factors and cell-based therapies.[9–12] For example, VEGFA is induced in infarct regions of the heart and is responsible for increased microvasculature permeability, granulation tissue thickness, and vessel formation.[13,14] VEGF receptors are expressed in ECs in the infarct region of mouse models post MI,[2] but the angiogenic response does not return myocardial health and function back to pre-MI levels, especially under diabetic conditions. The exact mechanisms limiting angiogenesis post MI remain poorly understood. However, impaired endothelial

Received 9 December 2022; accepted 17 May 2023;
https://doi.org/10.1016/j.omtn.2023.05.021.

[7]These authors contributed equally

Correspondence: Basak Icli, PhD, Molecular Cardiology Research Institute, Department of Medicine, Tufts Medical Center, Boston, MA 02111, USA.
E-mail: bicli@tuftsmedicalcenter.org

function resulting from diabetes or obesity could have important implications for this process.[15,16] While current therapies are aimed at limiting the damage the heart incurs post MI, there is a lack of available treatments that improve myocardial repair.[1]

The above observations suggest that additional factors may limit angiogenesis post MI and thus contribute to adverse remodeling post infarct. Many patients with coronary artery disease have concomitant conditions such as diabetes or obesity, which independently promote endothelial dysfunction and could therefore adversely affect angiogenesis.[15,16] Thus, understanding the mechanisms through which these metabolic conditions impair angiogenesis might identify potential candidate therapeutic targets not only to limit myocardial damage but to promote cardiac repair after MI.[1]

MicroRNAs (miRNAs) are small, non-protein-coding RNAs that are 19–25 nt in length that are capable of binding the 3′ untranslated region (UTR) of target mRNA through association with an RNA-induced silencing complex (RISC).[4] This binding leads to inhibition or degradation of the target mRNA, making miRNAs powerful regulators of gene expression with vast potential for therapeutic applications. miRNAs regulate numerous physiological and pathological cellular functions and have been implicated in the process of angiogenesis, including in the myocardium post MI.[15,17] We recently identified miR-409-3p as a regulator of angiogenesis in brown fat and as promoting insulin resistance with increased expression in the ECs of obese mouse brown adipose tissue (BAT).[18] As described above, metabolic conditions promote coronary artery disease and may contribute to insufficient angiogenesis after MI. Therefore, in the current study, we examined the regulation of miR-409-3p in the setting of patients with acute MI and in a mouse experimental MI model. We also investigated the molecular mechanisms in the EC through which miR-409-3p alters angiogenesis.

DNAJ heat shock protein family member B9 (DNAJB9) is a member of the molecular chaperone gene family, a group of specialized proteins that can bind to substrate proteins and assist with folding, unfolding, degradation, translocation, or disaggregation of protein aggregates. Although its exact function is not completely understood, DNAJB9 is known to act as a co-chaperone to major chaperone families, such as heat shock protein 70s (Hsp70).[19] DNAJB9 is also involved in the unfolded protein response (UPR), a highly conserved pathway that is classically activated by endoplasmic reticulum (ER) stress[20] and is transcriptionally activated when unfolded proteins accumulate in the ER lumen (ER stress). Other factors are also known to be involved in activation of the UPR pathway. Plasma levels of palmitate, a saturated free fatty acid, is increased in obesity or insulin resistance, adversely affecting many cellular processes and inducing low-level inflammation. Palmitate can activate the UPR in many cell types, resulting in associated ER stress.[21]

Here, we report that EC-specific deletion of miR-409-3p improves angiogenesis and heart function in mice post MI and targets the DNAJB9/p38 mitogen-activated protein kinase (MAPK) signaling pathway. These findings unveil possible targets for future therapeutic modulation to improve angiogenesis and remodeling of the heart post MI.

RESULTS

To investigate the regulatory role miR-409-3p may play in acute MI, miR-409-3p expression was measured in human plasma samples from the Feiring Heart Biopsy Study 2 in a cohort of 21 adult patients undergoing coronary bypass surgery (coronary artery bypass grafting [CABG]) with non-coronary syndrome (NCS) or those with MI or unstable angina within 30 days prior to admission. As seen in Figure 1A, circulating levels of miR-409-3p were increased by 83% in acute coronary syndrome (ACS) patient plasma samples, as measured by quantitative real-time PCR. Similarly, C57BL6/J wild-type (WT) mice that underwent left anterior descending (LAD) coronary artery ligation with 45-min ischemia followed by reperfusion showed increased circulating miR-409-3p compared with the sham surgery controls (Figure 1B). To elucidate regulation of miR-409-3p expression by pro-angiogenic factors, human umbilical vein ECs (HUVECs) were treated with the prototypical pro-angiogenic growth factors VEGF or FGF. Interestingly, while the pro-angiogenic growth factors VEGF and FGF significantly reduced miR-409-3p expression in HUVECs over 24 h (Figures 1C and 1D), palmitate significantly increased miR-409-3p expression over 24 h (Figure 1E). In summary, these data suggest that miR-409-3p is differentially regulated by pro- and anti-angiogenic stimuli and that its expression may correlate with acute ischemic injury.

Functionally, in the presence of palmitate, overexpression of miR-409-3p "mimics" (miR-409-3p$_m$) in HUVECs inhibited cell growth by 22%, whereas miR-409 inhibitors (miR-409$_i$, complementary antagonist) increased EC growth by 22.2% (Figure 2A). miR-409-3p overexpression in the presence of palmitate decreased wound closure in scratch assays by 33% compared with the non-specific (NS) control, whereas miR-409-3p inhibition increased wound closure by 39% compared with the NS control (Figures 2B and S1), suggesting that miR-409-3p retains its anti-angiogenic function in ECs in the presence of palmitate.

To identify a target of miR-409-3p, a systematic approach utilizing RNA sequencing (RNA-seq) profiling and *in silico* approaches combining bioinformatics with prediction algorithms such as miRGator and TargetScan was endeavored. RNA-seq analysis identified DNAJB9 as one of the top regulated genes from 32 genes that were repressed by at least a 1.4-fold change (FC) with false discovery rate (FDR)-adjusted $p < 0.01$ (Figure 3A). In accordance with our RNA-seq profiling approach, multiple independent prediction algorithms also identified DNAJB9 as a predicted target of miR-409-3p with two potential binding sites in the 3′ UTR (Figures S2A and S2B). Gene Ontology (GO) canonical pathway analyses, also performed utilizing genes' FDR-adjusted $p < 0.01$, predicted the UPR as the most significantly regulated pathway (Figure 3B). Interestingly, DNAJB9 is known to be a part of the UPR signaling pathway.[22] Furthermore, GO disease and function analyses predicted miR-409-3p to be

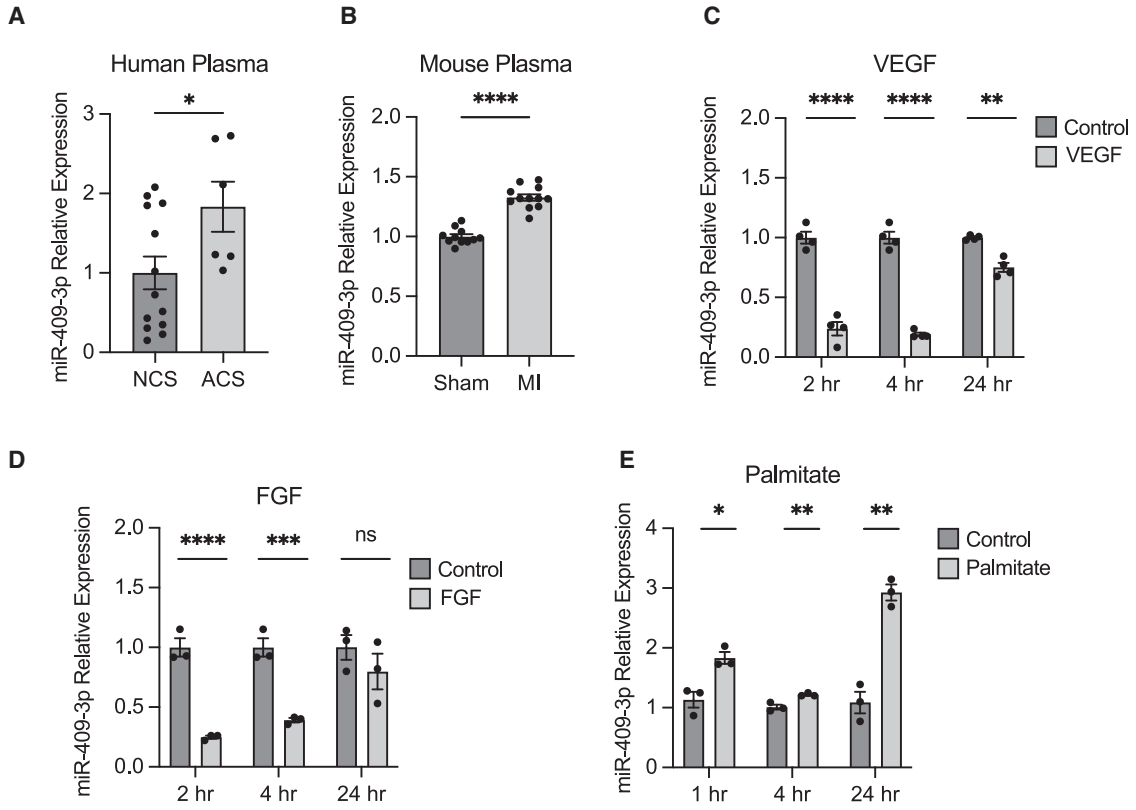

Figure 1. Expression of miR-409-3p in patients with ACS and in murine myocardial ischemia

(A and B) Expression of miR-409-3p in plasma of patients with ACS (A) and plasma of mice that underwent sham surgery or LAD ligation with 45-min ischemia-reperfusion (B). (C–E) Modulation of miR-409-3p expression in HUVECs treated with 50 ng/mL VEGF (C), 50 ng/mL FGF (D), or 100 μM palmitate (E). Data are representative of 3–6 replicates per condition unless indicated otherwise. Statistical significance was determined by unpaired Student's t test or two-way ANOVA. *p < 0.05, **p < 0.01, ***p < 0.001, ****p < 0.0001. Error bars indicate ± SEM.

involved in cellular growth and function (Figure 3C), in agreement with our findings *in vitro*. Overexpression of miR-409-3p decreased DNAJB9 mRNA expression by 47% compared with a NS control (Figure 3D) in the presence of palmitate, while DNAJB9 protein expression was decreased by 31.2% (Figure 3E, top). Conversely, inhibition of miR-409-3p increased DNAJB9 expression by 24.6% (Figure 3E, bottom). Argonaute2 (AGO2) microribonucleoprotein (miRNP) immunoprecipitation (IP) studies showed 1.9-fold enrichment of DNAJB9 (Figure 3F), while FEM1C, a gene that was not predicted by RNA-seq analysis to be a target of miR-409-3p, was not enriched in the presence of miR-409-3p (Figures S2C and S2D). Furthermore, overexpression of miR-409-3p inhibited luciferase activity of the reporter construct containing the 3′ UTR sequence of DNAJB9 (Figure 3G). Collectively, these data indicate that DNAJB9 is a *bona fide* target of miR-409-3p in ECs.

To identify downstream signaling pathways of miR-409-3p, we performed GO analyses using the differentially expressed genes (DEGs) with FC > 1.4 and FDR-adjusted p < 0.01 from the RNA-seq datasets. DEGs were subjected to GO network analysis, and p38 MAPK was among the significantly regulated signaling pathways (Figure 4A). Overexpression of miR-409-3p in ECs significantly reduced the p38 phosphorylation up to 29% in response to 30 and 60 min of palmitate stimulation (Figure 4B), whereas miR-409-3p inhibition increased p38 MAPK phosphorylation by up to 47% in response to 30 and 60 min of palmitate stimulation (Figure 4C). This regulation was specific to p38 signaling, while other signaling pathways, such as protein kinase B (AKT) or mammalian target of rapamycin (mTOR) were not found to be modulated by miR-409-3p (Figures S3A and S3B).

To determine whether DNAJB9 silencing can functionally recapitulate the effects of miR-409-3p in EC growth and migration, we employed the small interfering RNA (siRNA) knockdown strategy to silence DNAJB9 expression in ECs (Figure S2E). Silencing of DNAJB9 mimicked miR-409-3p′s effects on EC migration, as measured by wound healing scratch assay (Figure 5A), and inhibited EC growth in the presence of palmitate (Figure 5B), similar to miR-409-3p overexpression. Additionally, knockdown of DNAJB9 decreased p38 phosphorylation up to 25% after 60 and 90 min of palmitate stimulation (Figure 5C). Collectively, these data indicate that DNAJB9 knockdown phenocopies the effects of miR-409-3p in ECs.

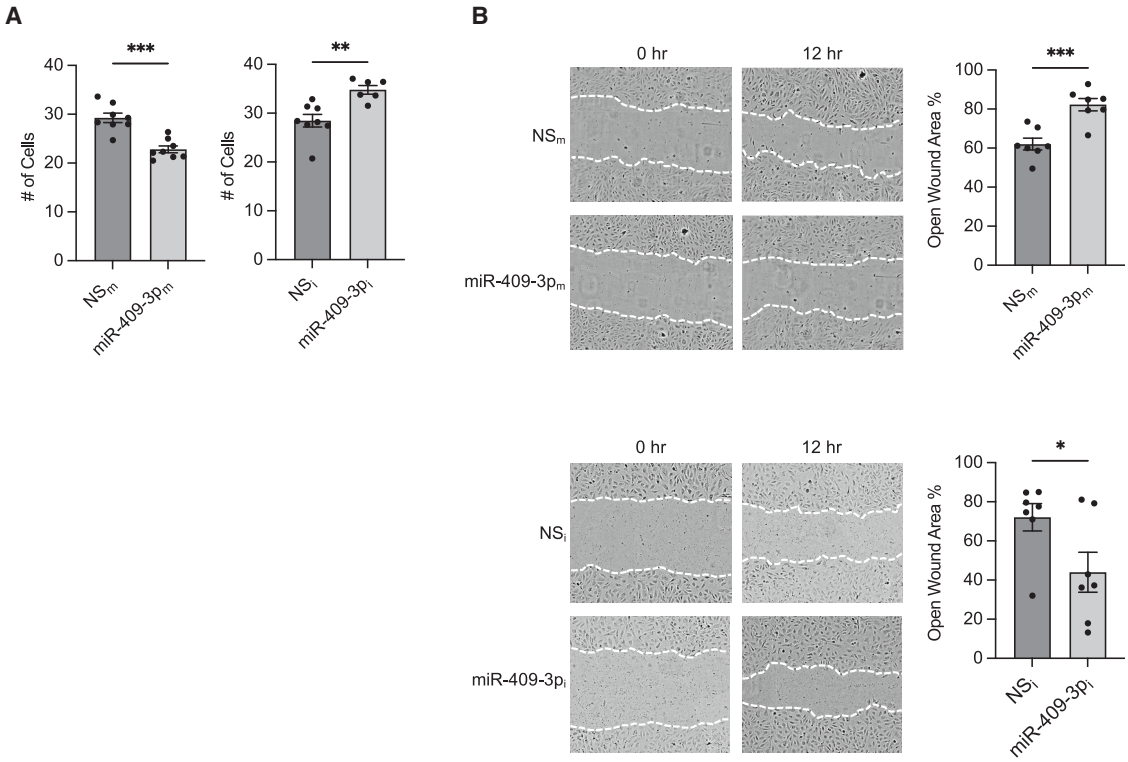

Figure 2. miR-409-3p modulates angiogenesis in ECs in the presence of palmitate

(A and B) Growth (A) and EC migration (B) assays in HUVECs transfected with NS control (NS_m) or miR-409-3p mimic (miR-409-$3p_m$) or miR-negative inhibitor control (NS_i) and miR-409-3p inhibitor (miR-409-$3p_i$) under 16-h 100 μM palmitate treatment. Statistical significance was determined by unpaired Student's t test and based on comparison with the respective control group. *$p < 0.05$, **$p < 0.01$, ***$p < 0.001$. ns, not significant. n = 6–8 replicates per condition. Error bars indicate ±SEM.

To study the EC-specific effects of miR-409-3p neutralization on MI, an EC-specific knockout mouse model of miR-409-3p was generated using homozygous *loxP* floxed mice (*miR409* $^{fl/fl}$) and crossed with mice with a constitutively active VE-Cadherin promoter to generate EC-specific miR-409-3p knockout (*miR409*^{ECKO}) mice (Figure S4A). Cre-mediated recombination was confirmed by genomic DNA PCR (Figure S4B). Compared with the *miR409* $^{fl/fl}$ control group, miR-409-3p expression in *miR409*^{ECKO} mice was reduced by 80% in ECs isolated from the heart but not in peripheral blood mononuclear cells (PBMCs) (Figure S4C). Additionally, miR-409-3p expression was reduced by 88% in ECs compared with the non-EC fraction of the heart (composed of ∼77% cardiac myocytes, 21% vascular smooth muscle cells, and 2% fibroblasts) in *miR409*^{ECKO} mice (Figure S4D). To assess whether EC-specific neutralization of miR-409-3p will induce angiogenesis and ameliorate LV function decline post acute MI, *miR409* $^{fl/fl}$ control mice and *miR409*^{ECKO} mice were fed a high-fat and high-sucrose diet for 8 weeks subjected to 45-min LAD ligation followed by reperfusion (Figure 6A). In response to the high-fat and high-sucrose diet, plasma free fatty acid (FFA) levels of *miR409* $^{fl/fl}$ and *miR409*^{ECKO} were increased by 37.9% and 38.3%, respectively, compared with the chow control group (Figure S4E). Transthoracic echocardiography was performed on mice prior to ischemia-reperfusion as well as 2 days post MI to evaluate LV function. Baseline ejection fraction (EF) and fractional shortening (FS) were normal. Furthermore, there were no significant differences in EF or FS in baseline echocardiograms of the *MiR409* $^{fl/fl}$ or the *MiR409*^{ECKO} group (Figure S5B). Infarct area was 33.8% smaller in the *MiR409*^{ECKO} compared to the control group as measured by triphenyltetrazolium chloride (TTC) staining of the heart (Figures 6B and S5A), while there were no significant changes observed in the heart weights or total body weights between the groups (Figure S5E). Short-axis M-mode echocardiogram images showed a 28% improvement in LV EF and a 23% improvement in FS in the *miR409*^{ECKO} group compared with the *miR409*$^{fl/f}$ control group 2 days post MI (Figures 6C and S5C). In addition, the *miR409*^{ECKO} group also showed a smaller change in EF and FS 2 days post MI compared with the baseline measurements (Figures 6C and S5C). In agreement with these findings, long axis B-mode echocardiogram images showed 32% improvement of the LV EF in the *miR409*^{ECKO} group compared with the *miR409*$^{fl/f}$ control group 2 days post MI (Figure S5D). To evaluate angiogenesis post MI, heart tissue was harvested 2 days post ischemia-reperfusion, and the border zone was stained for isolectin B4 and CD31. Interestingly, *miR409*^{ECKO} mice showed a 53.3% increase in isolectin B4 staining (Figure 6D), while CD31 was increased by 56% (Figure 6E), and elimination of the primary antibody did not result in a significant signal (Figure S5F).

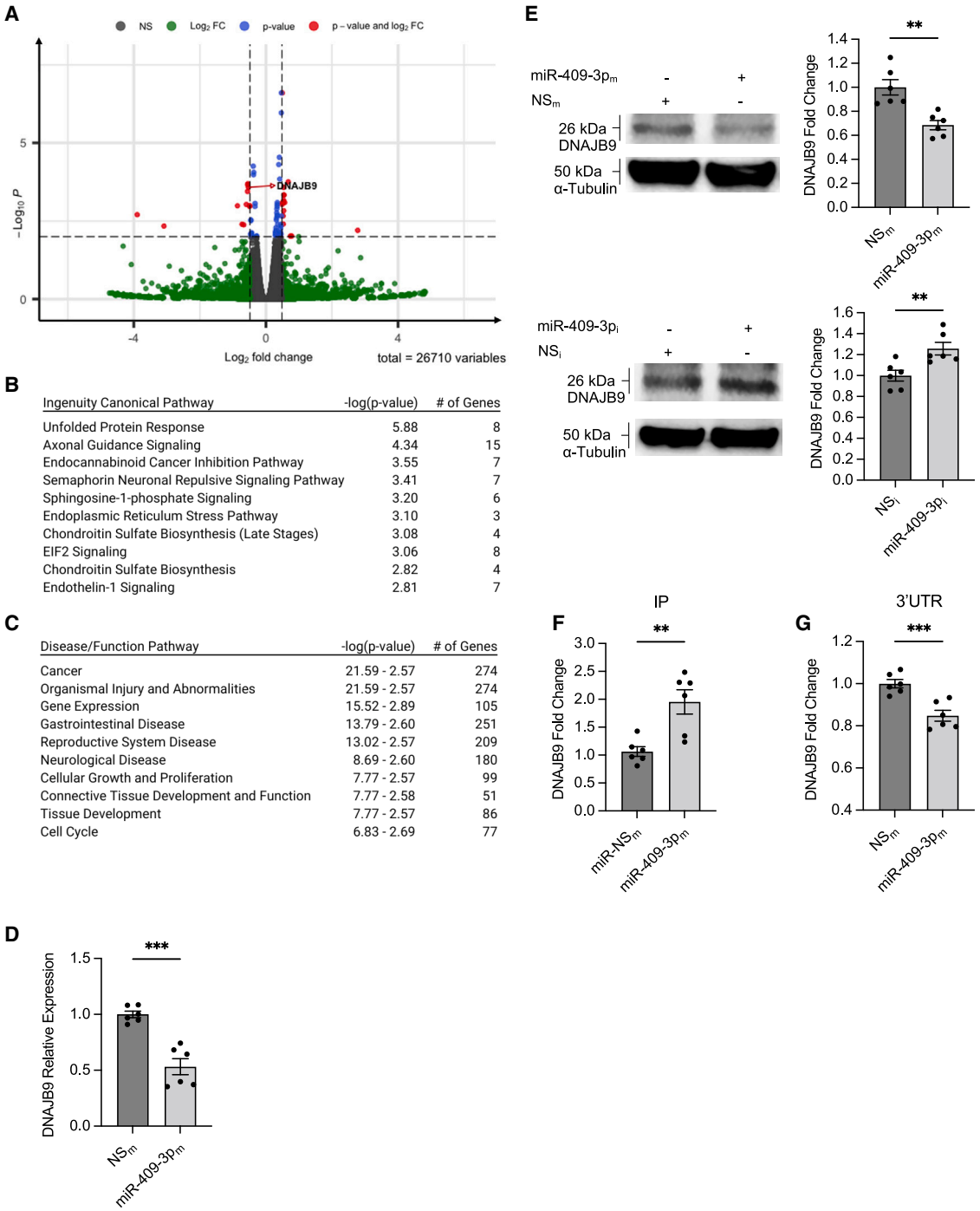

B

Ingenuity Canonical Pathway	-log(p-value)	# of Genes
Unfolded Protein Response	5.88	8
Axonal Guidance Signaling	4.34	15
Endocannabinoid Cancer Inhibition Pathway	3.55	7
Semaphorin Neuronal Repulsive Signaling Pathway	3.41	7
Sphingosine-1-phosphate Signaling	3.20	6
Endoplasmic Reticulum Stress Pathway	3.10	3
Chondroitin Sulfate Biosynthesis (Late Stages)	3.08	4
EIF2 Signaling	3.06	8
Chondroitin Sulfate Biosynthesis	2.82	4
Endothelin-1 Signaling	2.81	7

C

Disease/Function Pathway	-log(p-value)	# of Genes
Cancer	21.59 - 2.57	274
Organismal Injury and Abnormalities	21.59 - 2.57	274
Gene Expression	15.52 - 2.89	105
Gastrointestinal Disease	13.79 - 2.60	251
Reproductive System Disease	13.02 - 2.57	209
Neurological Disease	8.69 - 2.60	180
Cellular Growth and Proliferation	7.77 - 2.57	99
Connective Tissue Development and Function	7.77 - 2.58	51
Tissue Development	7.77 - 2.57	86
Cell Cycle	6.83 - 2.69	77

Figure 3. DNAJB9 is a target of miR-409-3p

(A) RNA-seq analyses of ECs that overexpress miR-409-3p or an NS control and treated with 100 μM palmitate with FDR-corrected $p < 0.01$ and fold change (FC) > 1.4. (B and C) GO analysis of RNA-seq with predicted (B) top 10 ingenuity canonical pathways and (C) disease/function pathways. (D and E) HUVECs transfected with NS_m or miR-409-3p_m or NS_i or miR-409-3p_i and treated with 100 μM palmitate for 16 h were subjected to (D) quantitative real-time PCR to measure DNAJB9 mRNA or (E) western blot analysis using antibodies to DNAJB9 and α-tubulin. (F) AGO2 miRNP IP quantitative real-time PCR analysis of enrichment of DNAJB9 mRNA in HUVECs transfected with NS_m or miR-409-3p_m and treated with 100 μM palmitate for 16 h. (G) Luciferase activity of the DNAJB9 3′ untranslated region (UTR) normalized to protein concentration was quantified in HEK293T cells transfected with NS_m or miR-409-3p_m. Statistical significance was determined by unpaired Student's t test or two-way ANOVA based on comparison with the respective NS control group. *$p < 0.05$, **$p < 0.01$, ***$p < 0.001$. n = 6 replicates per condition. Error bars indicate ± SEM.

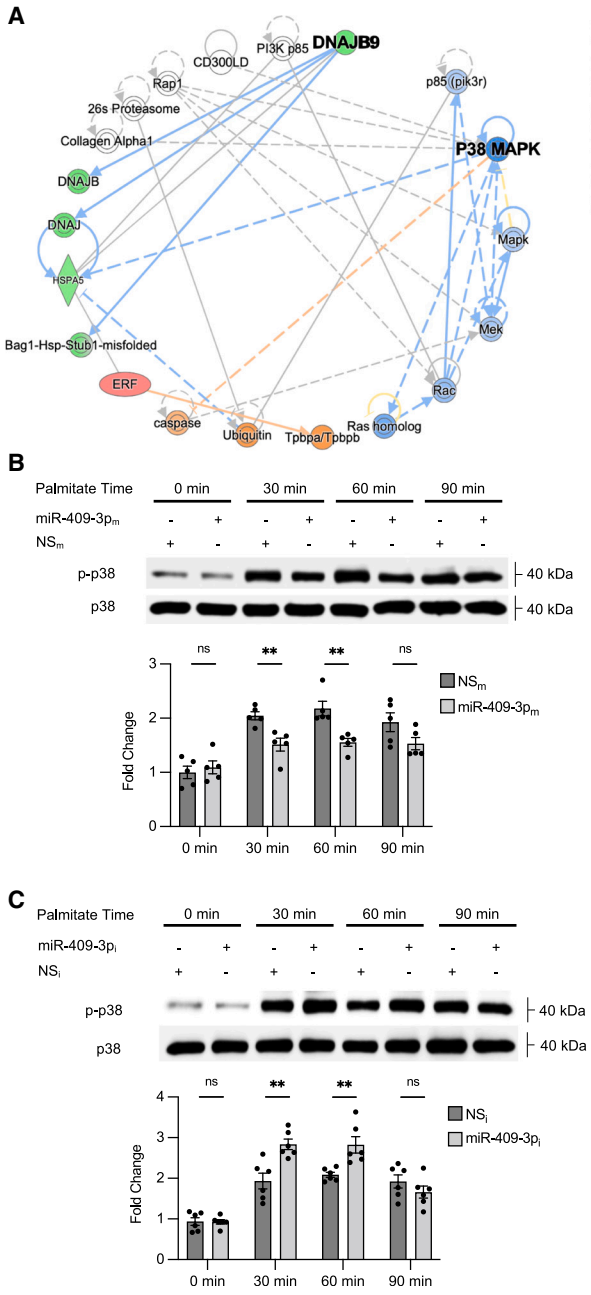

Kinase	Distance (Nodes)
PI3K p85	2
P38 MAPK	2
p85 (pik3r)	3
Mapk	3
Mek	3
Rac	3
Ras homolog	3

Figure 4. miR-409-3p modulates p38 MAPK signaling

(A) Gene network visualization of the RNA-seq date set from ECs overexpressing miR-409-3p or the NS control and treated with 100 μM palmitate for 16 h identified P38 MAPK as a potential downstream signaling pathway. (B and C) Western blot analyses of phosphorylated p38 (p-p38) and p38 antibodies on HUVECs transfected with NS_m or miR-409-$3p_m$ (B) and NS_i or miR-409-$3p_i$ (C) and treated with 100 μM palmitate for the indicated duration. Statistical significance was determined by unpaired Student's t test or two-way ANOVA based on a comparison with the respective NS control group. *$p < 0.05$, **$p < 0.01$. n = 5–6 replicates per condition. Error bars indicate ± SEM.

DISCUSSION

In the current study, we investigated the role of miR-409-3p in angiogenesis after MI. We observed the following: (1) there is increased circulating miR-409-3p in humans after ACS syndrome or in mice after ischemia/reperfusion; (2) miR-409-3p opposes endothelial migration and angiogenesis *in vitro*; (3) miR-409-3p modulates p38 MAPK pathway activation through direct targeting of DNAJB9; and (4) genetic deletion of endothelial miR-409-3p promotes angiogenesis and recovery of LV function after ischemia/reperfusion in mice. We interpret these findings to identify miR-409-3p as a novel regulator of post-MI angiogenesis through the DNAJB9-p38 MAPK signaling axis.

Acute MI remains one of the leading causes of death among ischemic cardiovascular diseases in the US and around the world. Myocardial healing after acute ischemia is a complex biological process, and accumulating studies demonstrate the importance of angiogenesis in post-MI healing and in improvement of LV function.[23–27] However, this process is markedly impaired in the context of insulin resistance and diabetes. In recent years, a number of miRNAs have been reported to potentially induce therapeutic angiogenesis post MI. For example, miR-26a has been characterized as an anti-angiogenic miRNA increased in MI that inhibits EC migration and sprouting angiogenesis through targeting bone morphogenic protein (BMP)/SMAD1 signaling,[17] whereas miR-210 has been found to promote angiogenesis in the myocardium post MI, leading to improved cardiac function through stimulating hepatocyte growth factor.[28] miR-92a is an anti-angiogenic miRNA that targets mRNAs corresponding to pro-angiogenic proteins and is inhibited by oxidative stress.[29] However, the exact mechanism by which these miRNAs modulate angiogenesis and the role of ECs in this process is not completely understood.[2,17,30,31]

Furthermore, in accordance with our *in vitro* findings, staining for DNAJB9 exhibited a 41.5% increase in response to EC-specific miR-409-3p neutralization in *miR409*^{ECKO} mice compared with the control group (Figure 6F) as well as a corresponding 2-fold increase in DNAJB9 expression level in the ischemic zone of the heart (Figure 6G), while phosphorylation of p38 MAPK was significantly increased 1.9-fold overall between the two groups (Figure 6H). In summary, these results identify an important role of miR-409-3p in improving LV function post MI through modulation of angiogenesis.

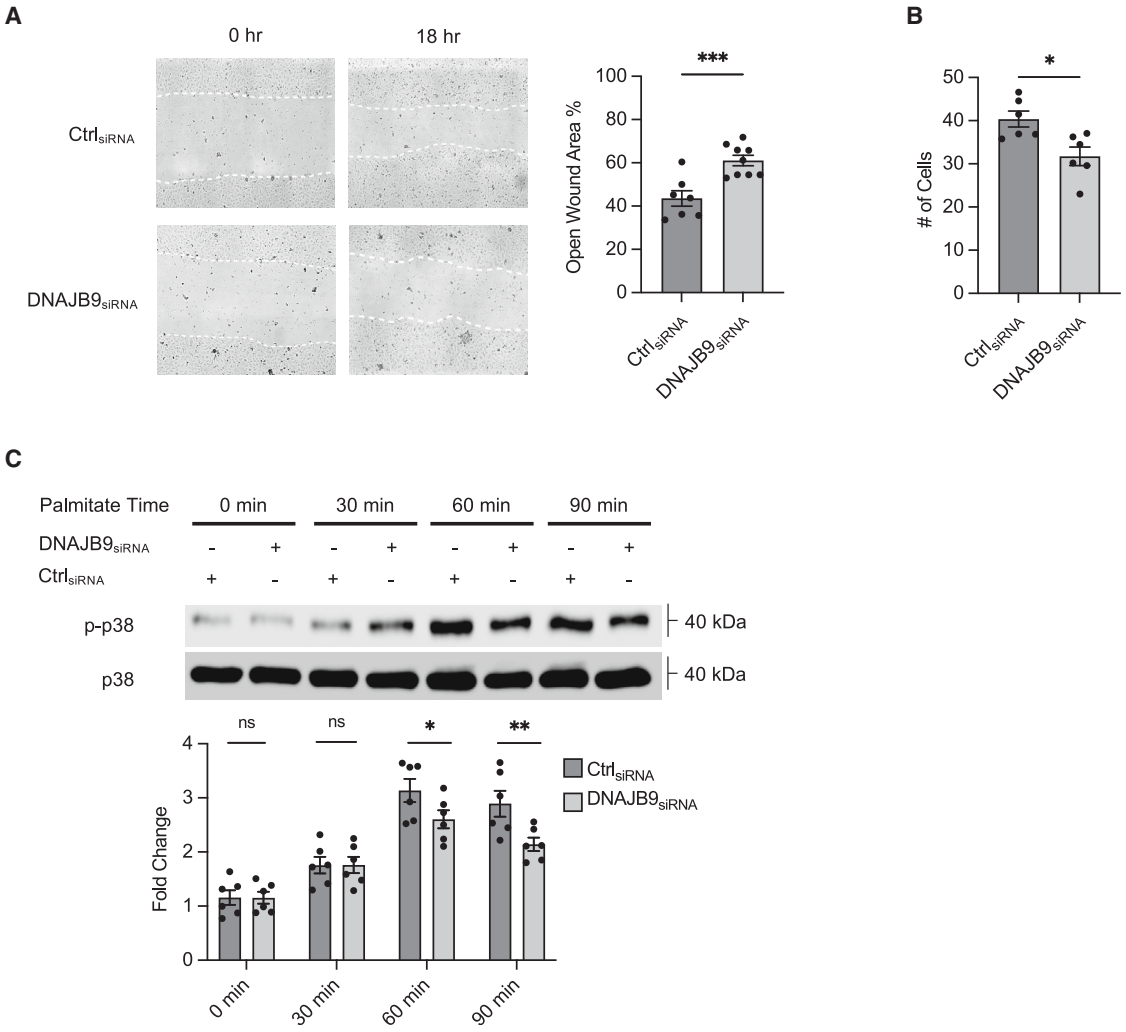

Figure 5. Knockdown of DNAJB9 functionally recapitulates miR-409-3p's effects *in vitro*

(A–C) EC migration (A), growth (B), and western blot analysis (C) of p38 MAPK signaling in HUVECs transfected with negative control siRNA ($Ctrl_{siRNA}$) or DNAJB9 siRNA ($DNAJB9_{siRNA}$). ECs were treated for 16–18 h with palmitate (A and B) or for the indicated duration (C). Statistical significance was determined by unpaired Student's t test or two-way ANOVA based on comparison with the indicated control group. *p < 0.05, **p < 0.01, ***p < 0.001. n = 6–9 replicates per condition. Error bars indicate ± SEM.

Our group recently identified miR-409-3p as an important regulator of adipose tissue angiogenesis, browning, and metabolism in obese mice.[18] However, its role in post-MI angiogenesis and heart function has not been studied before. In this investigation, we show that neutralization of endothelial miR-409-3p rapidly stimulates angiogenesis post MI by increasing DNAJB9 expression and p38 MAPK phosphorylation, building on the growing body of literature showing an important role of miRNAs in regulating the angiogenic response post MI. Furthermore, we identified that miR-409-3p expression is increased in response to acute MI in mice and in human subjects with ACS (Figures 1A and 1B). Overexpression of miR-409-3p impaired EC angiogenic responses in the presence of palmitate, while its inhibition had the opposite effects, solidifying its role as a potent anti-angiogenic miRNA (Figures 2 and S1). EC-specific genetic deletion of miR-409-3p in mice that consumed a high-fat and high-sucrose diet for 8 weeks showed robust induction of angiogenesis within 2 days of MI with improved LV function and reduced infarct size (Figures 6A–6F and S4A). It is important to note that we observed some variation in infarct size (Figure S5A), which may be caused by the slight variations of the mouse vascular anatomy as well as surgical variation during ligation of the LAD. However, the observed variation in our studies is in accordance with studies utilizing ischemia-reperfusion[32,33] or permanent LAD ligation models in mice.[34,35] Our findings suggest, for the first time, that deficiency of miR-409-3p improves LV function and angiogenesis in response to myocardial ischemia.

Vascular endothelium plays an important role in maintaining vascular homeostasis and regulates vascular tone, permeability, blood fluidity, inflammation, and angiogenesis.[36–38] Plasma FFA levels are

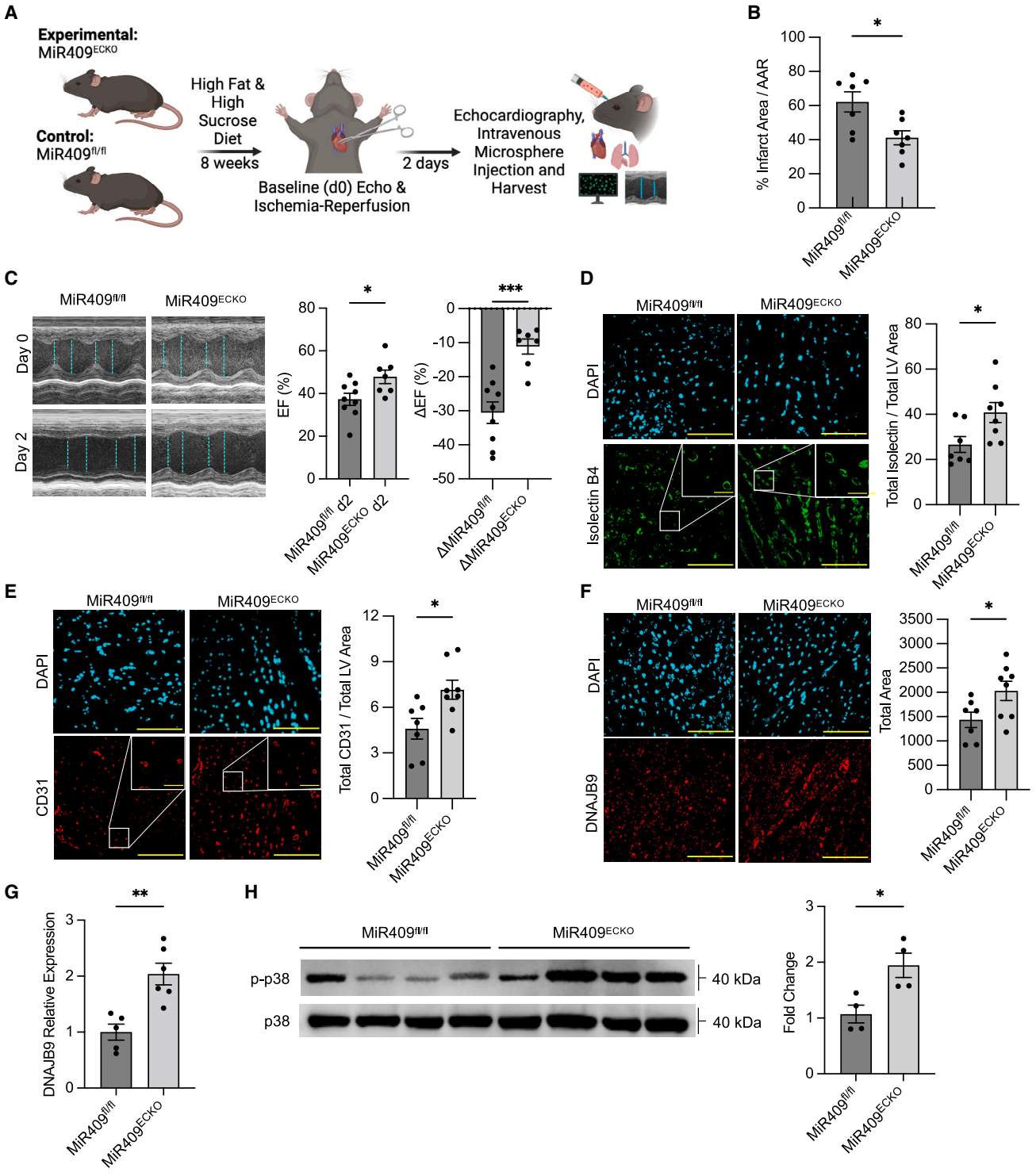

Figure 6. EC-specific knockout of miR-409-3p improves angiogenesis and heart function in a murine model of acute MI

(A) Ischemia-reperfusion injury was performed on *miR409*^{ECKO} and *miR409*$^{fl/fl}$ control mice after 8 weeks of a high-fat, high-sucrose diet. (B) Infarct size in the left ventricle was calculated with triphenyltetrazolium chloride (TTC) staining of the heart and normalized to the AAR. (C) Representative M-mode SAX echocardiograms, LV ejection fraction (EF), and difference from baseline data 2 days after ischemia-reperfusion injury. (D and E) Angiogenesis post MI was quantified on day 2 in heart sections from the border zone stained for isolectin B4 (D) or CD31 (E) (scale bars, 100 μm; inset, 12.5 μm). (F) DNAJB9 positivity in the border zone of the heart was measured by confocal microscopy (scale

(legend continued on next page)

increased in patients with type 2 diabetes (T2D) and obesity, resulting in increased prevalence of cardiovascular events.[39–42] An increasing number of studies show a correlation between FFAs and vascular endothelium dysfunction.[43,44] Additionally, miRNAs have been implicated in improving various aspects of palmitate-induced EC dysfunction, such as dampening inflammation, apoptosis, and stimulating EC migration.[45–49] Here, we used palmitate, a 16-carbon saturated fatty acid and a common circulating saturated FFA,[50] to dissect the role of miR-409-3p and its targets in EC-driven angiogenic responses. Interestingly, while palmitate increased miR-409-3p expression in ECs (Figure 1E), neutralization of miR-409-3p expression in ECs in the presence of palmitate significantly increased EC growth and migration (Figure 2), overcoming palmitate-induced EC dysfunction (Figure S1). DNAJB9 similarly phenocopied miR-409-3p′s effects on EC growth and migration in the presence of palmitate through regulation of p38 MAPK signaling (Figure 5). Mice with genetic EC deletion of miR-409-3p that were maintained on a high-fat and high-sucrose diet showed elevated plasma FFA levels comparable with the literature.[51,52] However, LV function and infarct size were improved in *miR409*^{ECKO} mice, suggesting alleviation of EC dysfunction caused by prolonged exposure to a Western diet. These findings are in agreement with the literature, where modulation of other miRNAs has been shown to improve palmitate-induced EC dysfunction.[53] For example, overexpression of miR-155 has been shown to inhibit palmitate-induced apoptosis and promote EC proliferation through regulation of the Wnt signaling pathway,[47] whereas miR-126 modulated EC migration through the ERK (extracellular signal-regulated kinase)/MAPK signaling axis in the presence of palmitate[49]; however, our study is distinct from others. First, we identified DNAJB9, a member of the UPR pathway, to be directly targeted by miR-409-3p to exert its downstream effects on regulation of EC angiogenesis. Next, we showed that the p38 MAPK signaling pathway was utilized by the miR-409-3p/DNAJB9 signaling axis in the presence of palmitate in ECs *in vitro* and in a genetic deletion of endothelial miR-409-3p in a mouse model of acute MI *in vivo*.

Investigative efforts to improve the prognosis of MI patients have centered around use of angiogenic or anti-apoptotic factors or cell-based therapies targeting the interface between perfused and non-perfused areas within the myocardium. Accumulating studies report the benefits of enhanced angiogenesis by increasing cardiomyocyte survival within the ischemic zone and subsequent LV function.[10,23–26] We examined angiogenesis within the ischemic zone in our genetic deletion of endothelial miR-409-3p in a mouse model that underwent LAD ligation with 45-min ischemia-reperfusion and showed that this non-perfused area is an active site of angiogenesis as early as 2 days after MI. Consistent with previous reports, confocal immunofluorescence evaluation of the border zone showed increased angiogenesis, as measured by CD31 and isolectin B4 staining (Figure 6). Furthermore, the increase in angiogenesis positively correlated with improved LV function, as measured by EF and FS (Figures 6 and S5). One of the mechanisms explaining the increased angiogenesis observed in *miR409*^{ECKO} mice may involve activation of p38 MAPK through DNAJB9 (Figures 5 and 6). Activation of p38 MAPK has been shown to induce actin organization and endothelial migration.[54] Pharmacological inhibition of p38 MAPK in an experimental prostate tumor model *in vivo* was associated with a significant reduction in tumor growth and vessel density, an effect that was associated with pathological angiogenesis.[55] Our studies are in agreement with these findings, where neutralization of miR-409-3p in ECs increased EC migration *in vitro* in the presence of palmitate (Figure 2). Additionally, overexpression of miR-409-3p or siRNA knockdown of DNAJB9 significantly decreased EC migration (Figures 2 and 5).

There are a few limitations of this study. First, our *in vivo* experiments involved a non-inducible, constitutively active, genetic deletion of miR-409-3p. We observed that ECs isolated from the heart of this mouse strain showed an ∼80% decrease in miR-409-3p expression (Figure S4C, left). Although the remaining miR-409-3p expression could be due to slight contamination of non-ECs, such as fibroblasts, cardiac myocytes, or other cell types that also express miR-409-3p,[18] it could also be the result of incomplete recombination. The UPR pathway has been shown by several groups[56,57] to have cardioprotective effects following ischemia-reperfusion injury. Therefore, we cannot completely rule out involvement of non-EC cell types in the phenotype reported in this study. In total PBMCs, we did not observe a difference in miR-409-3p expression between Cre+ *miR409*^{ECKO} mice and their littermate Cre− *MiR409* $^{fl/fl}$ controls, ruling out a possible contribution from immune cells (Figure S4C, right). We further profiled expression of miR-409-3p in Cre+ *miR409*^{ECKO} mice and showed an ∼89% decrease in miR-409-3p expression in ECs compared with non-ECs. In an effort to profile the relative expression of miR-409-3p in non-EC heart extracts, we measured miR-409-3p expression in the major cardiac cell types, as documented in the literature.[58,59] While ∼77% of the non-EC cell population obtained was composed of cardiac myocytes, ∼21% vascular smooth muscle cells, and 2% fibroblasts. Therefore, a significant majority of miR-409-3p expression in the non-EC heart extracts was contributed by cardiac myocytes (Figure S4D).

We note that the canonical UPR involves a sophisticated set of signaling pathways that are activated when altered cellular homeostatic conditions disrupt protein folding in the ER, causing accumulation of unfolded/misfolded proteins, which, in turn, leads to activation of the UPR pathway.[60] Increased ER stress and the UPR are known to have downstream angiogenic effects. For example, Hsp70 is highly expressed in ECs and regulates EC proliferation, survival, and migration in tumor angiogenesis.[61] Interestingly, angiogenic stimuli, such as hypoxia, ischemia, inflammation, and oxidative stress, can also trigger the UPR pathway, and this process has been

bars, 100 μm). (G) Relative mRNA expression levels of DNAJB9 in the ischemic zone. (H) Western blot analysis of the p38 MAPK signaling pathway from ischemic zone heart samples (n = 4 mice per group). Statistical significance was determined by unpaired Student's t test or two-way ANOVA based on comparison with the indicated control group. *$p < 0.05$, **$p < 0.01$, ***$p < 0.001$. n = 5–8 mice per condition unless noted otherwise. Error bars indicate ±SEM.

Table 1. Primers for quantitative real-time PCR

Gene	Forward sequence (5′-3′)	Reverse sequence (5′-3′)	Species
β-Actin	GGACTTCGAGCAAGAGATGG	AGCACTGTGTTGGCGTACAG	human
HPRT	GCTATAAATTCTTTGCTGACCTGCTG	AATTACTTTTATGTCCCCTGTTGACTGG	human
DNAJB9	TCTTAGGTGTGCCAAAATCGG	TGTCAGGGTGGTACTTCATGG	human
DNAJB9	CTCCACAGTCAGTTTTCGTCTT	GGCCTTTTTGATTTGTCGCTC	mouse
MYC	GGCTCCTGGCAAAAGGTA	CTGCGTAGTTGTGTGCTGATGT	human
β-Actin	GAAATCGTGCGTGACATCAAAG	TGTAGTTTCATGGATGCCACAG	mouse
TNNT2	CAGAGGAGGCCAACGTAGAAG	CTCCATCGGGGATCTTGGGT	mouse
ACTA2	GTCCCAGACATCAGGGAGTAA	TCGGATACTTCAGCGTCAGGA	mouse
DDR2	ATCACAGCCTCAAGTCAGTGG	TTCAGGTCATCGGGTTGCAC	mouse
vWF	CTCTTTGGGGACGACTTCATC	TCCCGAGAATGGAGAAGGAAC	mouse

shown to be vital for endothelial survival and activity. Furthermore, molecular chaperones that normally facilitate protein folding in the ER can regulate angiogenic factor production and angiogenic responses.[61–64] In this report, we showed that one of these chaperone molecules, DNAJB9,[65] facilitates EC-mediated angiogenic responses in the heart following MI through regulation of p38 MAPK signaling. There are several upstream ER transmembrane protein sensors in the canonical UPR pathway that mediate UPR signals, such as inositol-requiring 1 (IRE1), PKR-like ER kinase (PERK), and activating transcription factor 6 (ATF6), which, in turn, activate transcription factors such as XBP1 (X-box binding protein 1). Nuclear translocation of XBP1 induces expression of ER chaperones such as DNAJB9 and calreticulin (CALR)[66] to alleviate ER stress and prevent chronic UPR activation.[60] In addition, in ECs, UPR can be activated without accumulation of unfolded proteins in the ER, a pathway that is associated with VEGF activation of the mTORC1 complex through the UPR mediators IRE1, PERK, and ATF6.[22] Our studies are novel and add to these findings by showing that, in the presence of palmitate, miR-409-3p modulates DNAJB9 expression, which, in turn, regulates p38 MAPK phosphorylation and angiogenesis. However, whether such regulation requires ER stress involving the IRE/XBP1 signaling node or through ER stress-independent activation of UPR signaling by palmitate remains to be determined.

Despite some of the limitations discussed here, the novel mechanistic insights from this study have important implications. We demonstrated here, for the first time, that miR-409-3p is dysregulated after MI and plays an important role in promoting EC angiogenic processes and the ischemic angiogenic response to acute MI. Identification of DNAJB9 as a novel miR-409-3p target provides potential clues regarding the mechanism by which miR-409-3p modulates EC angiogenic responses. EC-specific knockout of miR-409-3p in our genetic *miR409*^{ECKO} mouse strain shows that there is a significant increase in phosphorylation of p38 MAPK signaling, a pathway that modulates EC migration.[54] These findings support the mechanism by which miR-409-3p modulates angiogenesis through utilization of the UPR in ECs and provide new opportunities for therapeutic intervention.

MATERIALS AND METHODS

Cell culture and transfection

HUVECs (Lonza, CC-2519) passaged fewer than five times were used for all experiments and cultured in EGM-2 growth medium (Lonza, cc-3162). For transfection studies, HUVECs plated at 50,000 cells/mL were cultured overnight before being transfected with Lipofectamine 2000 transfection reagent (Invitrogen, 52887) in accordance with the manufacturer's instructions. For reporter studies, HUVECs were transfected with 400 ng of the indicated reporter constructs and either 50 nM miR-409-3p mimic (Thermo Scientific, 4464066) or NS control (Thermo Scientific, 4464058) or 100 nM miR-409-3p inhibitor (Thermo Scientific, 4464084) or NS control (Thermo Scientific, 4464076). All knockdown experiments were conducted using the same transfection protocol with the respective control (Thermo Scientific, 4390843) or target of interest siRNA at 30 nM, except for the scratch EC migration assay at 10 nM.

Quantitative real-time PCR

HUVECs were suspended in TRIzol reagent (Invitrogen), and total RNA and miRNA were isolated according to the manufacturer's instructions. Reverse transcriptions were performed using the QIAGEN QuantiTect Reverse Transcription Kit (205311) or miRCURY LNA RT Kit (339340). The QuantiTect SYBR Green RT-PCR Kit (204245) or miRCURY LNA SYBR Green PCR Kit (339345) from QIAGEN, respectively, was used for quantitative real-time PCR analysis with the CFX Opus 96 real-time PCR system (Bio-Rad). Gene-specific primers (Invitrogen) were used to detect human DNAJB9, while specific miRCURY LNA miRNA PCR assays from QIAGEN (339306) were used to detect miR-409-3p (Table 1). Samples were normalized to either endogenous human β-actin or 5S rRNA. FCs were calculated by ΔΔCt method. Significance was determined by Student's two-tailed t test or one-way ANOVA; $p < 0.05$.

Western blot analysis

HUVECs transfected with miR-409-3p mimic, miR-409-3p inhibitor, NS miR controls, DNAJB9 siRNA, or control siRNA were cultured for 72 h before the cells were harvested. Mouse tissue was harvested

according to the experimental protocol, and a mechanical tissue homogenizer was used. Total cellular protein was isolated by RIPA buffer (50 mM Tris-HCl [pH 7.4], 150 mM NaCl, 1% NP-40, 0.5% sodium deoxycholate, and 0.1% SDS; Boston BioProducts, BP-115) supplemented with 1× Halt protease inhibitor cocktail (Thermo Scientific, 1861261) and 1× 0.5 M EDTA (Thermo Scientific, 1861274). Cell or tissue debris was removed by centrifugation at 15,000 rpm for 15 min. Protein quantification was performed using the Pierce BCA Protein Assay Kit (Thermo Scientific, 23227). Lysates were separated using 5%–15% gels, transferred to polyvinylidene fluoride (PVDF) membranes, and subjected to western blotting using antibodies against DNAJB9 (Abcam, ab118282). phosphorylated p38 (p-p38; Cell Signaling Technology, 9215), p38 MAPK (Cell Signaling Technology, 9212), p-AKT (Cell Signaling Technology, 4060), pan-AKT (Cell Signaling Technology, 2920), p-mTOR (Cell Signaling Technology, 2971), mTOR (Cell Signaling Technology, 2972), α-tubulin (Cell Signaling Technology, 3873), and β-actin (Cell Signaling Technology, 4970) were incubated with gentle agitation at 4°C overnight at a concentration of 1:1,000. Horseradish peroxidase (HRP)-conjugated goat anti-rabbit antibody (Cell Signaling Technology, 7074) at a dilution of 1:2,000, HRP-conjugated horse anti-mouse antibody (Cell Signaling Technology, 7076) at a 1:5,000 dilution, or HRP-conjugated mouse anti-goat antibody (Santa Cruz Biotechnology, sc-2354) at a 1:2,000 dilution were used, depending on the primary antibody specifications. An enhanced chemiluminescence (ECL) assay was performed according to the manufacturer's instructions (Thermo Scientific, 34095, A38555). Three or more biological replicates were performed for each experiment. Quantification was conducted using ImageJ software, and significance was determined by Student's two-tailed t test or one-way ANOVA; $p < 0.05$.

Total RNA extraction and bulk RNA-seq analysis

Total RNA from HUVECs transfected with 30 nM miR-409-3p mimic or NS control and treated with 100 μM palmitate was purified using the RNeasy Mini Kit (QIAGEN, 74104). The library preparation was done using the QIAseq Stranded mRNA Kit (QIAGEN). From 500 ng starting material, the mRNA was enriched and fragmented using enzymatic fragmentation. After first and second strand synthesis, the cDNA was end repaired and 3′ adenylated. Sequencing adapters were ligated to the overhangs. Adapted molecules were enriched using 13 cycles of PCR and purified by bead-based cleanup. The library size distribution was validated and quality inspected on a TapeStation (Agilent Technologies). Libraries are pooled based in equimolar concentrations based on the Bioanalyzer automated electrophoresis system (Agilent Technologies). The library pools were quantified using qPCR, and an optimal concentration of the library pool was used to generate clusters on the surface of a flow cell before sequencing on a NextSeq500/550 instrument (1× 75 cycles) according to the manufacturer's instructions (Illumina). Raw data from RNA-seq were deposited into GEO: GSE231988.

Pathway enrichment analysis

DEGs were identified using adjusted $p < 0.01$ (FDR) and $FC > 1.3$. The DEGs were visualized using a volcano plot generated with EnhancedVolcano R package (GitHub). DEGs were also subjected to network analysis using Ingenuity Pathway Analysis (IPA) software (QIAGEN). Genes that were identified with $p < 0.05$ were subjected to gene set enrichment analyses using IPA software (QIAGEN). The significant values for the canonical pathways were calculated by Fisher's exact test, and the top 10 pathways were visualized.

miRNP IP

miRNP IP was performed as described previously.[67] Briefly, Myc-tagged Ago-2 was co-transfected with either miR-409-3p or miR negative control in HUVECs. Cells were washed in ice-cold PBS, released by scraping, and lysed in buffer (10 mM Tris-HCl [pH 7.5], 10 mM NaCl, 2 mM EDTA, 0.5% Triton X-100, 100 units/mL of RNase Plus [Promega] supplemented with 1× protease inhibitor. One-twentieth of the supernatant volume was collected in TRIzol for use as an extract control. The remaining portion of the supernatant was pre-cleared with protein A/G UltraLink Resin (Pierce), to which 2 μg anti c-myc antibody (Cell Signaling Technology, 2276) was added, and the mixture was allowed to incubate overnight at 4°C. The following day, protein A/G UltraLink Resin was added. After 4 h of mechanical rotation at 4°C, the agarose beads were pelleted and washed four times in wash buffer (50 mM Tris-HCl [pH 7.5], 150 mM NaCl, 0.05% Triton X-100). Finally, 1 mL of TRIzol was added to the beads, and RNA was isolated as described above. Total RNA was reverse transcribed into cDNA for quantitative real-time PCR analysis.

Scratch assay for EC migration

HUVECs plated in 12-well plates at 50,000 cells/well and transfected with miR-409-3p mimic, miR-409-3p inhibitor, NS miR controls, DNAJB9 siRNA, or control siRNA were cultured for 60 h in 12-well plates. The cell monolayer was scratched using a 200-μL micropipette tip to form a 750-μm wound, followed by 16–18 h of 100 μM palmitate treatment. Cells were imaged by a CytoSMART Omni live-cell imaging device (CytoSMART Technologies) over time to assess wound closure. 3–5 technical replicates were used per condition.

EC growth assay

HUVECs transfected with miR-409-3p mimic, miR-409-3p inhibitor, NS miR controls, DNAJB9 siRNA, or control siRNA were cultured for 24 h in 12-well plates. Cells were then plated in 24-well plates at 8,000 cells/well and treated with 100 μM palmitate for 16 h, followed by tagging with Calcein AM (Thermo Scientific, C3100) at 1 μM for 1 h at 37°C. Imaging was performed using Nikon FL and LI-COR Odyssey M and analyzed using ImageJ software to assess cell growth. Four technical replicates and 7 random images were taken blindly per condition.

Histology and immunostaining

Murine heart tissues were embedded in paraffin and sectioned. Sections were deparaffinized and rehydrated, and antigen retrieval was done by placing the slides in 10 mM Tris at 85°C for 30 min. Blocking was performed using 5% normal donkey serum (Jackson ImmunoResearch,

017-000-121) with 0.2% Triton X-100 for 90 min at room temperature. Streptavidin/biotin blocking (Vector Laboratories, SP-2002) was performed on sections to be stained for isolectin B4. Sections were incubated with primary antibodies overnight at 4°C. Primary antibodies were diluted in 5% normal donkey serum with 0.2% Triton X-100 as follows: 1:25 goat pAb to DNAJB9 (Abcam, ab118282), 1:25 rat anti-CD31 (Dianova, DIA-310), and 1:100 biotinylated isolectin B4 (Vector Laboratories, B-1205). Slides were washed with PBS and incubated with the secondary antibodies DyLight594 horse anti-goat IgG (Vector Laboratories, DI-3094), Cy3-conjugated AffiniPure donkey anti-rat IgG (Jackson ImmunoResearch, 712-165-153), or Alexa Fluor 488-conjugated streptavidin (Jackson ImmunoResearch, 016-540-084), respectively, for 90 min at room temperature. After drying, slides were mounted with ProLong Gold antifade reagent with DAPI (Invitrogen, P36935). Quantification was performed using ImageJ software from 6 random areas obtained by confocal imaging using Olympus FV3000. Hematoxylin and eosin (H&E)-stained heart sections were imaged using LI-COR Odyssey M, and total LV area quantification was performed using ImageJ software.

TTC staining and fluorescent microsphere injections

Mice were injected with 75μL of 2-μm FluoSpheres carboxylate-modified microspheres (F8826, Thermo Scientific) retro-orbitally 48 h post ischemia-reperfusion. The harvested heart was sliced into 2-mm sections using heart slicer matrix. Each slice was used to quantify the area at risk (AAR) and the infarcted zone. The AAR, demarcated by fluorescent microspheres, was visualized using LI-COR Odyssey M. To outline the infarcted area, sections were incubated in 1% (w/v) TTC (Sigma) in PBS (pH 7.4) at 37°C for 20 min. For each section, the AAR and infarct area were measured using ImageJ.

Luciferase activity assay and cell culture transfection

DNAJB9 3′ UTR (OriGene, SC214927) sequences were PCR amplified with specific primers and purified, followed by restriction enzyme digestion. HEK293T cells (a gift from the MCRI Cell Culture Core) cultured in 12-well plates were transfected in triplicates using Lipofectamine 2000 transfection reagent with 500 ng of the indicated reporter construct per well. After 24 h, cells were transfected with 50 nM miR-409-3p mimic and the equivalent NS control. Cells were then harvested 12 h later in accordance with the Luciferase Reporter Assay System (Promega, E4530). Each reading of luciferase activity was normalized to the total protein read for the same lysate as quantified using the Pierce BCA Protein Assay Kit (Thermo Scientific, 23227).

Experimental ischemia-reperfusion model

MI was performed as described previously.[68] Briefly, 12-week-old mice were deeply anesthetized and ventilated, and the heart was exposed through a thoracotomy. A suture was tied around the proximal LAD artery for 45 min, after which the suture was untied, and the chest was closed.

Transthoracic echocardiography and analyses

Mice were anesthetized with 2.5% isoflurane, and short-axis (SAX) M-mode images and long-axis (LAX) B-mode images were acquired through transthoracic echocardiography before ischemia-reperfusion and 48 h after ischemia-reperfusion. Analyses were performed using the Vevo LAB 3.1.0 (Fujifilm) cardiac package. EF and FS were measured by averaging values obtained from 5 cardiac cycles in SAX M-mode and from B-mode LAX images as described previously.[69,70] SAX M-mode images were obtained at the mid-papillary level, with care taken to measure only endocardium not overlapping with the papillary muscles.

EC isolation from the heart

Hearts were harvested 48 h post ischemia-reperfusion and digested with 1 mg/mL collagenase and dispase solution in DMEM/F12 at 37°C for 40 min, followed by neutralization with DMEM/F12 with 10% fetal bovine serum (FBS). The cell suspension was filtrated through a 70-μm strainer (BD Falcon) and centrifuged at 500 × *g* for 10 min at 4°C. The resulting pellet was suspended in RBC lysis solution (eBioscience) for 5 min and neutralized with DMEM/F12 medium with 10% FBS. The suspension was then filtered through a 40-μm strainer (BD Falcon), and the pellet was suspended in PBS with 0.1% BSA and 2 mM EDTA. Later, the suspension was incubated with sheep anti-rat IgG Dynabeads coated with PECAM-1 antibodies (BD Biosciences, 557,355). The bead-bound cells were collected using a magnet and washed 3 times. The composition of the non-EC cell lysates was evaluated using the following primer sets: TNNT2 (Troponin T2, cardiac type) for cardiac myocytes, DDR2 (discoidin domain receptor tyrosine kinase 2) for fibroblasts, ACTA2 (actin alpha 2, smooth muscle) for vascular smooth muscle cells, and vWF (von Willebrand factor) for ECs (Table 1).

PBMC isolation

Murine blood from heart puncture was heparinized and pooled to 2 mice per sample. Lymphocyte separation media (LSM) 1107 (PromoCell, C-44010) was used according to the manufacturer's instructions with 3 mL LSM per blood sample. PBMCs were washed with PBS three times. The centrifugation step post first wash was repeated twice to form a pellet. After three washes, cells were resuspended in 1 mL TRIzol.

FFA analysis

Blood was extracted from mice collected in K2EDTA-coated tubes (BD Microtainer, 365974) and immediately centrifuged at 2,000 × *g* for 10 min. The plasma supernatant was collected and stored at −80°C for later use. Measurement of non-esterified fatty acids (NEFAs) in plasma by a coupled enzymatic reaction system was conducted using the FFA Assay Kit (Fluorometric), which contains palmitic acid as a standard (Cell Biolabs, STA-619). The FFA assay was performed as instructed by the manufacturer, and 1:5-diluted plasma samples were used. The assay was performed on black 96-well plates (Brandplates, 781668), and fluorescence was detected by fluorescence microplate reader (Thermo Scientific, Varioskan LUX).

Animal studies

C57BL/6 homozygous floxed miR-409 mice (bearing *loxP* sites flanking the only exon of the miR-409 gene; Figure S4A) were generated at

Table 2. Primers for Cre/lox recombination and PCR genotyping

PCR primer set 1	5′arm forward F1: 5′-CGACCAGCATTTCATCCCGTTTAC-3′	3′*loxP* reverse R1: 5′-CTATACGAAGTTATTCTTCCCTGAG-3′
PCR primer set 2	5′*loxP* forward F2: 5′-ACGTAAACGGCCACAAGTTC-3′	3′arm reverse R2: 5′-GTTGGAAGAGCATTTTGCTGCTG-3′

Cyagen. Mice bearing the floxed allele were then crossed with constitutive Cre-expressing mice (kindly provided by Iris Z. Jaffe), resulting in EC-specific miR-409-3p-deficient mice (*miR409*^{ECKO}) and miR-409-3p$^{fl/fl}$ Cre^{-} littermates (*miR409* $^{fl/fl}$). The genotypes of mice were confirmed by PCR genotyping of tail biopsies (Transnetyx) using the indicated primers (Table 2).

Male, 4-week-old *miR409*^{ECKO} and *miR409* $^{fl/fl}$ mice were placed on a high-fat and high-sucrose diet containing 36 kcal % fat and 43.2 kcal % sucrose (Research Diets, D11092103) and maintained on a 12-h light/dark cycle in a pathogen-free animal facility for 8 weeks. Food was changed on a weekly basis in accordance with the manufacturer's guidelines, and animals had constant access to food and water. At the endpoint, all tissues and blood were harvested in accordance with Tufts University Institutional Animal Care and use (IACUC) standards, and tissues were either snap-frozen for RNA and protein isolation or fixed in 10% formalin (Sigma-Aldrich, HT5014) for histology. Blood was collected into EDTA tubes, and plasma was separated by 15-min 1,500 × *g* centrifugation, followed by RNA isolation using the Norgen RNA Purification Kit (17200) according to the manufacturer's instructions. Male mice were age matched in all experiments, and cage-matched littermates were used for experiments. Analyses of *in vivo* samples were performed by blinded observers. Animal protocols were approved by Laboratory Animal Care at Harvard Medical School and conducted in accordance with National Institutes of Health guidelines for proper care and use of laboratory animals.

Circulating miR-409-3p levels in patients with ACS

We examined EDTA plasma from a subgroup of 21 patients from the Feiring Heart Biopsy Study 2, which included adult patients undergoing CABG in the Feiring Heart Clinic in Norway between 2011 and 2017. The ACS diagnosis was defined as ACS in medical records. The study was approved by the Regional Ethics Committee in Norway. Written informed consent was obtained from participants or their appropriate surrogates. Plasma samples were generated from fasting blood collected in EDTA-containing containers before CABG and stored in small aliquots at −86°C. No thawing of the specimens was allowed prior to the actual RNA analyses. The Norgen RNA Purification kit (17200) was used to isolate RNA from the plasma samples according to the manufacturer's instructions, followed by reverse transcription and quantitative real-time PCR as described under Quantitative real-time PCR).

Statistical analysis

Data are presented as mean ± SEM. All *in vitro* and *in vivo* experiments are representative of 3 independent experiments unless indicated otherwise. Sample sizes for mouse experiments were chosen based upon pilot or similar well-characterized studies in the literature. There were no inclusion or exclusion criteria used. Data were subjected to unpaired two-sided Student's t-test, one-way ANOVA with Bonferroni correction for multiple comparisons, or two-way ANOVA with Šidák's multiple-comparisons test. $p < 0.05$ was considered statistically significant.

DATA AVAILABILITY

The data generated from this study and the associated resources are available from the corresponding author upon reasonable request.

SUPPLEMENTAL INFORMATION

Supplemental information can be found online at https://doi.org/10.1016/j.omtn.2023.05.021.

ACKNOWLEDGMENTS

We thank Megan Zhu for assistance with immunofluorescence staining, Prionti Talukdar for LV area measurements, and Nathan Li and the Tufts Comparative Pathology Services Animal Histology Core for histology services. This work was supported by American Diabetes Association grant 1-16-JDF-046 (to B.I.); a National Institutes of Health grant HL149999 (to B.I.); National Institutes of Health grants HL115141, HL134849, HL148207, HL148355, and HL153356 (to M.W.F.); American Heart Association grants 18SFRN33900144 and 20SFRN35200163 (to M.W.F.), National Institutes of Health grant HL-162919 (to R.M.B.), and the Harold Williams, MD, Medical Student Research Fellowship (to C.F.).

AUTHOR CONTRIBUTIONS

B.I. designed the research. F.B., C.F., K.L., C.E.N., G.F.G., G.L.M., R.P.-G., D.B.-G., J.W., and B.I. carried out the experiments. I.H., I.R., S.E.R., L.H.S., and M.W.F. contributed critical reagents. F.B., C.F., R.M.B., and B.I. analyzed and interpreted the data. F.B., C.F., and B.I.wrote the manuscript.

DECLARATION OF INTERESTS

The authors have declared that no conflicts of interest exist with this work.

REFERENCES

1. Li, J., Zhao, Y., and Zhu, W. (2022). Targeting angiogenesis in myocardial infarction: novel therapeutics (Review). Exp. Ther. Med. *23*, 64. https://doi.org/10.3892/etm.2021.10986.

2. Wu, X., Reboll, M.R., Korf-Klingebiel, M., and Wollert, K.C. (2021). Angiogenesis after acute myocardial infarction. Cardiovasc. Res. *117*, 1257–1273. https://doi.org/10.1093/cvr/cvaa287.

3. Ibanez, B., James, S., Agewall, S., Antunes, M.J., Bucciarelli-Ducci, C., Bueno, H., Caforio, A.L.P., Crea, F., Goudevenos, J.A., Halvorsen, S., et al. (2017). ESC Guidelines for the management of acute myocardial infarction in patients presenting with ST-segment elevation: the Task Force for the management of acute myocardial infarction in patients presenting with ST-segment elevation of the European Society of Cardiology (ESC). Eur. Heart J. *39*, 119–177. https://doi.org/10.1093/eurheartj/ehx393.

4. Wang, W., and Zheng, H. (2021). Myocardial infarction: the protective role of MiRNAs in myocardium Pathology. Front. Cardiovasc. Med. *8*, 631817. https://doi.org/10.3389/fcvm.2021.631817.

5. Fadini, G.P., Albiero, M., Bonora, B.M., and Avogaro, A. (2019). Angiogenic abnormalities in diabetes mellitus: mechanistic and clinical aspects. J. Clin. Endocrinol. Metab. *104*, 5431–5444. https://doi.org/10.1210/jc.2019-00980.

6. Jansson, P.A. (2007). Endothelial dysfunction in insulin resistance and type 2 diabetes. J. Intern. Med. *262*, 173–183. https://doi.org/10.1111/j.1365-2796.2007.01830.x.

7. Greer, J.J.M., Ware, D.P., and Lefer, D.J. (2006). Myocardial infarction and heart failure in the db/db diabetic mouse. Am. J. Physiol. Heart Circ. Physiol. *290*, H146–H153. https://doi.org/10.1152/ajpheart.00583.2005.

8. Carmeliet, P., and Jain, R.K. (2011). Molecular mechanisms and clinical applications of angiogenesis. Nature *473*, 298–307. https://doi.org/10.1038/nature10144.

9. Hedman, M., Hartikainen, J., Syvänne, M., Stjernvall, J., Hedman, A., Kivelä, A., Vanninen, E., Mussalo, H., Kauppila, E., Simula, S., et al. (2003). Safety and feasibility of catheter-based local intracoronary vascular endothelial growth factor gene transfer in the prevention of postangioplasty and in-stent restenosis and in the treatment of chronic myocardial ischemia: phase II results of the Kuopio Angiogenesis Trial (KAT). Circulation *107*, 2677–2683. https://doi.org/10.1161/01.CIR.0000070540.80780.92.

10. Kobayashi, K., Maeda, K., Takefuji, M., Kikuchi, R., Morishita, Y., Hirashima, M., and Murohara, T. (2017). Dynamics of angiogenesis in ischemic areas of the infarcted heart. Sci. Rep. *7*, 7156. https://doi.org/10.1038/s41598-017-07524-x.

11. Henry, T.D., Annex, B.H., McKendall, G.R., Azrin, M.A., Lopez, J.J., Giordano, F.J., Shah, P.K., Willerson, J.T., Benza, R.L., Berman, D.S., et al. (2003). The VIVA trial: vascular endothelial growth factor in Ischemia for Vascular Angiogenesis. Circulation *107*, 1359–1365. https://doi.org/10.1161/01.cir.0000061911.47710.8a.

12. Kukuła, K., Chojnowska, L., Dąbrowski, M., Witkowski, A., Chmielak, Z., Skwarek, M., Kądziela, J., Teresińska, A., Małecki, M., Janik, P., et al. (2011). Intramyocardial plasmid-encoding human vascular endothelial growth factor A165/basic fibroblast growth factor therapy using percutaneous transcatheter approach in patients with refractory coronary artery disease (VIF-CAD). Am. Heart J. *161*, 581–589. https://doi.org/10.1016/j.ahj.2010.11.023.

13. Vestweber, D. (2015). How leukocytes cross the vascular endothelium. Nat. Rev. Immunol. *15*, 692–704. https://doi.org/10.1038/nri3908.

14. Nahrendorf, M., Swirski, F.K., Aikawa, E., Stangenberg, L., Wurdinger, T., Figueiredo, J.L., Libby, P., Weissleder, R., and Pittet, M.J. (2007). The healing myocardium sequentially mobilizes two monocyte subsets with divergent and complementary functions. J. Exp. Med. *204*, 3037–3047. https://doi.org/10.1084/jem.20070885.

15. Perez-Cremades, D., Chen, J., Assa, C., and Feinberg, M.W. (2022). MicroRNA-mediated control of myocardial infarction in diabetes. Trends Cardiovasc. Med. https://doi.org/10.1016/j.tcm.2022.01.004.

16. Marfella, R., Esposito, K., Nappo, F., Siniscalchi, M., Sasso, F.C., Portoghese, M., Di Marino, M.P., Baldi, A., Cuzzocrea, S., Di Filippo, C., et al. (2004). Expression of angiogenic factors during acute coronary syndromes in human type 2 diabetes. Diabetes *53*, 2383–2391. https://doi.org/10.2337/diabetes.53.9.2383.

17. Icli, B., Wara, A.K.M., Moslehi, J., Sun, X., Plovie, E., Cahill, M., Marchini, J.F., Schissler, A., Padera, R.F., Shi, J., et al. (2013). MicroRNA-26a regulates pathological and physiological angiogenesis by targeting BMP/SMAD1 signaling. Circ. Res. *113*, 1231–1241. https://doi.org/10.1161/CIRCRESAHA.113.301780.

18. Becker-Greene, D., Li, H., Perez-Cremades, D., Wu, W., Bestepe, F., Ozdemir, D., Niosi, C.E., Aydogan, C., Orgill, D.P., Feinberg, M.W., and Icli, B. (2021). MiR-409-3p targets a MAP4K3-ZEB1-PLGF signaling axis and controls brown adipose tissue angiogenesis and insulin resistance. Cell. Mol. Life Sci. *78*, 7663–7679. https://doi.org/10.1007/s00018-021-03960-1.

19. Houry, W.A. (2001). Chaperone-assisted protein folding in the cell cytoplasm. Curr. Protein Pept. Sci. *2* (3), 227–244. https://doi.org/10.2174/1389203013381134.

20. Zhang, L., Zhang, C., and Wang, A. (2016). Divergence and conservation of the major UPR branch IRE1-bZIP signaling pathway across eukaryotes. Sci. Rep. *6*, 27362. https://doi.org/10.1038/srep27362.

21. Haywood, J., and Yammani, R.R. (2016). Free fatty acid palmitate activates unfolded protein response pathway and promotes apoptosis in meniscus cells. Osteoarthritis Cartilage *24*, 942–945. https://doi.org/10.1016/j.joca.2015.11.020.

22. Karali, E., Bellou, S., Stellas, D., Klinakis, A., Murphy, C., and Fotsis, T. (2014). VEGF Signals through ATF6 and PERK to promote endothelial cell survival and angiogenesis in the absence of ER stress. Mol. Cell *54*, 559–572. https://doi.org/10.1016/j.molcel.2014.03.022.

23. Cochain, C., Channon, K.M., and Silvestre, J.S. (2013). Angiogenesis in the infarcted myocardium. Antioxid Redox Signal. *18*, 1100–1113. https://doi.org/10.1089/ars.2012.4849.

24. Fazel, S., Cimini, M., Chen, L., Li, S., Angoulvant, D., Fedak, P., Verma, S., Weisel, R.D., Keating, A., and Li, R.K. (2006). Cardioprotective c-kit+ cells are from the bone marrow and regulate the myocardial balance of angiogenic cytokines. J. Clin. Invest. *116*, 1865–1877. https://doi.org/10.1172/JCI27019.

25. Fukuda, S., Kaga, S., Sasaki, H., Zhan, L., Zhu, L., Otani, H., Kalfin, R., Das, D.K., and Maulik, N. (2004). Angiogenic signal triggered by ischemic stress induces myocardial repair in rat during chronic infarction. J. Mol. Cell. Cardiol. *36*, 547–559. https://doi.org/10.1016/j.yjmcc.2004.02.002.

26. Sasaki, T., Fukazawa, R., Ogawa, S., Kanno, S., Nitta, T., Ochi, M., and Shimizu, K. (2007). Stromal cell-derived factor-1alpha improves infarcted heart function through angiogenesis in mice. Pediatr. Int. *49*, 966–971. https://doi.org/10.1111/j.1442-200X.2007.02491.x.

27. Li, N., Rignault-Clerc, S., Bielmann, C., Bon-Mathier, A.C., Déglise, T., Carboni, A., Ducrest, M., and Rosenblatt-Velin, N. (2020). Increasing heart vascularisation after myocardial infarction using brain natriuretic peptide stimulation of endothelial and WT1(+) epicardial cells. Elife *9*, e61050. https://doi.org/10.7554/eLife.61050.

28. Fan, Z.G., Qu, X.L., Chu, P., Gao, Y.L., Gao, X.F., Chen, S.L., and Tian, N.L. (2018). MicroRNA-210 promotes angiogenesis in acute myocardial infarction. Mol. Med. Rep. *17*, 5658–5665. https://doi.org/10.3892/mmr.2018.8620.

29. Li, S., Yuan, L., Su, L., Lian, Z., Liu, C., Zhang, F., Cui, Y., Wu, M., and Chen, H. (2020). Decreased miR92a3p expression potentially mediates the proangiogenic effects of oxidative stressactivated endothelial cellderived exosomes by targeting tissue factor. Int. J. Mol. Med. *46*, 1886–1898. https://doi.org/10.3892/ijmm.2020.4713.

30. Dai, Y., Yan, T., and Gao, Y. (2020). Silence of miR-32-5p promotes endothelial cell viability by targeting KLF2 and serves as a diagnostic biomarker of acute myocardial infarction. Diagn. Pathol. *15*, 19. https://doi.org/10.1186/s13000-020-00942-y.

31. Bonauer, A., Carmona, G., Iwasaki, M., Mione, M., Koyanagi, M., Fischer, A., Burchfield, J., Fox, H., Doebele, C., Ohtani, K., et al. (2009). MicroRNA-92a controls angiogenesis and functional recovery of ischemic tissues in mice. Science *324*, 1710–1713. https://doi.org/10.1126/science.1174381.

32. Noyan-Ashraf, M.H., Momen, M.A., Ban, K., Sadi, A.M., Zhou, Y.Q., Riazi, A.M., Baggio, L.L., Henkelman, R.M., Husain, M., and Drucker, D.J. (2009). GLP-1R agonist liraglutide activates cytoprotective pathways and improves outcomes after experimental myocardial infarction in mice. Diabetes *58*, 975–983. https://doi.org/10.2337/db08-1193.

33. Andersson, L., Scharin Täng, M., Lundqvist, A., Lindbom, M., Mardani, I., Fogelstrand, P., Shahrouki, P., Redfors, B., Omerovic, E., Levin, M., et al. (2015). Rip2 modifies VEGF-induced signalling and vascular permeability in myocardial ischaemia. Cardiovasc. Res. *107*, 478–486. https://doi.org/10.1093/cvr/cvv186.

34. Li, X., Redfors, B., Sáinz-Jaspeado, M., Shi, S., Martinsson, P., Padhan, N., Scharin Täng, M., Borén, J., Levin, M., and Claesson-Welsh, L. (2020). Suppressed vascular leakage and myocardial edema improve outcome from myocardial infarction. Original research. Front. Physiol. *2020*, 11. https://doi.org/10.3389/fphys.2020.00763.

35. Li, M., Yamada, S., Shi, A., Singh, R.D., Rolland, T.J., Jeon, R., Lopez, N., Shelerud, L., Terzic, A., and Behfar, A. (2021). Brachyury engineers cardiac repair competent stem cells. Stem Cells Transl Med. *10*, 385–397. https://doi.org/10.1002/sctm.20-0193.

36. Chlopicki, S. (2015). Perspectives in pharmacology of endothelium: from bench to bedside. Pharmacol. Rep. *67*. vi-ix. https://doi.org/10.1016/j.pharep.2015.08.005.

37. Aird, W.C. (2003). Endothelial cell heterogeneity. Crit. Care Med. *31* (4 Suppl), S221–S230. https://doi.org/10.1097/01.CCM.0000057847.32590.C1.

38. Lai, W.K.C., and Kan, M.Y. (2015). Homocysteine-induced endothelial dysfunction. Ann. Nutr. Metab. *67*, 1–12. https://doi.org/10.1159/000437098.

39. Wang, Y., Qian, Y., Fang, Q., Zhong, P., Li, W., Wang, L., Fu, W., Zhang, Y., Xu, Z., Li, X., and Liang, G. (2017). Saturated palmitic acid induces myocardial inflammatory injuries through direct binding to TLR4 accessory protein MD2. Nat. Commun. *8*, 13997. https://doi.org/10.1038/ncomms13997.

40. Pilz, S., Scharnagl, H., Tiran, B., Seelhorst, U., Wellnitz, B., Boehm, B.O., Schaefer, J.R., and März, W. (2006). Free fatty acids are independently associated with all-cause and cardiovascular mortality in subjects with coronary artery disease. J. Clin. Endocrinol. Metab. *91*, 2542–2547. https://doi.org/10.1210/jc.2006-0195.

41. Pilz, S., and März, W. (2008). Free fatty acids as a cardiovascular risk factor. Clin. Chem. Lab. Med. *46*, 429–434. https://doi.org/10.1515/CCLM.2008.118.

42. Shramko, V.S., Polonskaya, Y.V., Kashtanova, E.V., Stakhneva, E.M., and Ragino, Y.I. (2020). The short overview on the relevance of fatty acids for human cardiovascular disorders. Biomolecules *10*, 1127.

43. Egan, B.M., Greene, E.L., and Goodfriend, T.L. (2001). Nonesterified fatty acids in blood pressure control and cardiovascular complications. Curr. Hypertens. Rep. *3*, 107–116. https://doi.org/10.1007/s11906-001-0021-y.

44. Boden, G. (2008). Obesity and free fatty acids. Endocrinol Metab. Clin. N. Am. *37*, 635–646. https://doi.org/10.1016/j.ecl.2008.06.007.

45. Zheng, C., Zhang, J., Chen, X., Zhang, J., Ding, X., You, X., Fan, L., Chen, C., and Zhou, Y. (2019). MicroRNA-155 mediates obesity-induced renal inflammation and dysfunction. Inflammation *42*, 994–1003. https://doi.org/10.1007/s10753-019-00961-y.

46. Deng, H., Chu, X., Song, Z., Deng, X., Xu, H., Ye, Y., Li, S., Zhang, Q., Sun, C., and Li, Y. (2017). MicroRNA-1185 induces endothelial cell apoptosis by targeting UVRAG and KRIT1. Cell. Physiol. Biochem. *41*, 2171–2182. https://doi.org/10.1159/000475571.

47. Zhao, Y., Rao, W., Wan, Y., Yang, X., Wang, G., Deng, J., Dai, M., and Liu, Q. (2019). Overexpression of microRNA-155 alleviates palmitate-induced vascular endothelial cell injury in human umbilical vein endothelial cells by negatively regulating the Wnt signaling pathway. Mol. Med. Rep. *20*, 3527–3534. https://doi.org/10.3892/mmr.2019.10623.

48. Wang, Y., Wang, F., Wu, Y., Zuo, L., Zhang, S., Zhou, Q., Wei, W., Wang, Y., and Zhu, H. (2015). MicroRNA-126 attenuates palmitate-induced apoptosis by targeting TRAF7 in HUVECs. Mol. Cell. Biochem. *399*, 123–130. https://doi.org/10.1007/s11010-014-2239-4.

49. Wang, Y., Wang, M., Yu, P., Zuo, L., Zhou, Q., Zhou, X., and Zhu, H. (2020). MicroRNA-126 modulates palmitate-induced migration in HUVECs by downregulating myosin light chain kinase via the ERK/MAPK pathway. Front. Bioeng. Biotechnol. *8*, 913. https://doi.org/10.3389/fbioe.2020.00913.

50. Bollu, L.R., Katreddy, R.R., Blessing, A.M., Pham, N., Zheng, B., Wu, X., and Weihua, Z. (2015). Intracellular activation of EGFR by fatty acid synthase dependent palmitoylation. Oncotarget *6*, 34992–35003. https://doi.org/10.18632/oncotarget.5252.

51. Murray, A.J., Panagia, M., Hauton, D., Gibbons, G.F., and Clarke, K. (2005). Plasma free fatty acids and peroxisome proliferator-activated receptor alpha in the control of myocardial uncoupling protein levels. Diabetes *54*, 3496–3502. https://doi.org/10.2337/diabetes.54.12.3496.

52. Terauchi, Y., Takamoto, I., Kubota, N., Matsui, J., Suzuki, R., Komeda, K., Hara, A., Toyoda, Y., Miwa, I., Aizawa, S., et al. (2007). Glucokinase and IRS-2 are required for compensatory beta cell hyperplasia in response to high-fat diet-induced insulin resistance. J. Clin. Invest. *117*, 246–257. https://doi.org/10.1172/jci17645.

53. Gu, X., Wang, X.Q., Lin, M.J., Liang, H., Fan, S.Y., Wang, L., Yan, X., Liu, W., and Shen, F.X. (2019). Molecular interplay between microRNA-130a and PTEN in palmitic acid-mediated impaired function of endothelial progenitor cells: effects of metformin. Int. J. Mol. Med. *43*, 2187–2198. https://doi.org/10.3892/ijmm.2019.4140.

54. Rousseau, S., Houle, F., Landry, J., and Huot, J. (1997). p38 MAP kinase activation by vascular endothelial growth factor mediates actin reorganization and cell migration in human endothelial cells. Oncogene *15*, 2169–2177. https://doi.org/10.1038/sj.onc.1201380.

55. Rajashekhar, G., Kamocka, M., Marin, A., Suckow, M.A., Wolter, W.R., Badve, S., Sanjeevaiah, A.R., Pumiglia, K., Rosen, E., and Clauss, M. (2011). Pro-inflammatory angiogenesis is mediated by p38 MAP kinase. J. Cell. Physiol. *226*, 800–808. https://doi.org/10.1002/jcp.22404.

56. Glembotski, C.C., Rosarda, J.D., and Wiseman, R.L. (2019). Proteostasis and beyond: ATF6 in ischemic disease. Trends Mol. Med. *25*, 538–550. https://doi.org/10.1016/j.molmed.2019.03.005.

57. Zhou, Y., Wan, X., Seidel, K., Zhang, M., Goodman, J.B., Seta, F., Hamburg, N., and Han, J. (2021). Aging and hypercholesterolemia differentially affect the unfolded protein response in the vasculature of ApoE(-/-) mice. J. Am. Heart Assoc. *10*, e020441. https://doi.org/10.1161/JAHA.120.020441.

58. Banerjee, I., Fuseler, J.W., Price, R.L., Borg, T.K., and Baudino, T.A. (2007). Determination of cell types and numbers during cardiac development in the neonatal and adult rat and mouse. Am. J. Physiol. Heart Circ. Physiol. *293*, H1883–H1891. https://doi.org/10.1152/ajpheart.00514.2007.

59. Litviňuková, M., Talavera-López, C., Maatz, H., Reichart, D., Worth, C.L., Lindberg, E.L., Kanda, M., Polanski, K., Heinig, M., Lee, M., et al. (2020). Cells of the adult human heart. Nature *588*, 466–472. https://doi.org/10.1038/s41586-020-2797-4.

60. Kaufman, R.J., and Cao, S. (2010). Inositol-requiring 1/X-box-binding protein 1 is a regulatory hub that links endoplasmic reticulum homeostasis with innate immunity and metabolism. EMBO Mol. Med. *2*, 189–192. https://doi.org/10.1002/emmm.201000076.

61. Dong, D., Stapleton, C., Luo, B., Xiong, S., Ye, W., Zhang, Y., Jhaveri, N., Zhu, G., Ye, R., Liu, Z., et al. (2011). A critical role for GRP78/BiP in the tumor microenvironment for neovascularization during tumor growth and metastasis. Cancer Res. *71*, 2848–2857. https://doi.org/10.1158/0008-5472.CAN-10-3151.

62. Ozawa, K., Tsukamoto, Y., Hori, O., Kitao, Y., Yanagi, H., Stern, D.M., and Ogawa, S. (2001). Regulation of tumor angiogenesis by oxygen-regulated protein 150, an inducible endoplasmic reticulum chaperone. Cancer Res. *61*, 4206–4213.

63. Wouters, B.G., van den Beucken, T., Magagnin, M.G., Koritzinsky, M., Fels, D., and Koumenis, C. (2005). Control of the hypoxic response through regulation of mRNA translation. Semin. Cell Dev. Biol. *16*, 487–501. https://doi.org/10.1016/j.semcdb.2005.03.009.

64. Zhang, S.X., Ma, J.H., Bhatta, M., Fliesler, S.J., and Wang, J.J. (2015). The unfolded protein response in retinal vascular diseases: implications and therapeutic potential beyond protein folding. Prog. Retin. Eye Res. *45*, 111–131. https://doi.org/10.1016/j.preteyeres.2014.12.001.

65. Yoshida, H., Matsui, T., Yamamoto, A., Okada, T., and Mori, K. (2001). XBP1 mRNA is induced by ATF6 and spliced by IRE1 in response to ER stress to produce a highly active transcription factor. Cell *107*, 881–891. https://doi.org/10.1016/s0092-8674(01)00611-0.

66. Salati, S., Genovese, E., Carretta, C., Zini, R., Bartalucci, N., Prudente, Z., Pennucci, V., Ruberti, S., Rossi, C., Rontauroli, S., et al. (2019). Calreticulin Ins5 and Del52 mutations impair unfolded protein and oxidative stress responses in K562 cells expressing CALR mutants. Sci. Rep. *9*, 10558. https://doi.org/10.1038/s41598-019-46843-z.

67. Sun, X., Icli, B., Wara, A.K., Belkin, N., He, S., Kobzik, L., Hunninghake, G.M., Vera, M.P.; MICU Registry, and Blackwell, T.S., et al. (2012). MicroRNA-181b regulates NF-kappaB-mediated vascular inflammation. J. Clin. Invest. *122*, 1973–1990. https://doi.org/10.1172/JCI61495.

68. Jin, H., Welzig, C.M., Aronovitz, M., Noubary, F., Blanton, R., Wang, B., Rajab, M., Albano, A., Link, M.S., Noujaim, S.F., et al. (2017). QRS/T-wave and calcium alternans in a type I diabetic mouse model for spontaneous postmyocardial infarction ventricular tachycardia: a mechanism for the antiarrhythmic effect of statins. Heart Rhythm *14*, 1406–1416. https://doi.org/10.1016/j.hrthm.2017.05.026.

69. Richards, D.A., Aronovitz, M.J., Calamaras, T.D., Tam, K., Martin, G.L., Liu, P., Bowditch, H.K., Zhang, P., Huggins, G.S., and Blanton, R.M. (2019). Distinct phenotypes induced by three degrees of transverse aortic constriction in mice. Sci. Rep. *9*, 5844. https://doi.org/10.1038/s41598-019-42209-7.

70. Zacchigna, S., Paldino, A., Falcão-Pires, I., Daskalopoulos, E.P., Dal Ferro, M., Vodret, S., Lesizza, P., Cannatà, A., Miranda-Silva, D., Lourenço, A.P., et al. (2021). Towards standardization of echocardiography for the evaluation of left ventricular function in adult rodents: a position paper of the ESC Working Group on Myocardial Function. Cardiovasc. Res. *117*, 43–59. https://doi.org/10.1093/cvr/cvaa110.